Fast Murine Airway Segmentation and Reconstruction in Micro-CT Images

Xabier Artaechevarria[a], Arrate Muñoz-Barrutia[a], Bram van Ginneken[b] and Carlos Ortiz-de-Solórzano[a]

[a]Center for Applied Medical Research, University of Navarra, 31008 Pamplona, Spain;
[b]Image Sciences Institute, 3584CX Utrecht, The Netherlands

ABSTRACT

Mouse models are becoming instrumental for the study of lung disease. Due to its resolution and low cost, high resolution Computed Tomography (micro-CT) is a very adequate technology to visualize the mouse lungs *in-vivo*. Automatic segmentation and measurement of airways in micro-CT images of the lungs can be useful as a preliminary step prior other image analysis quantification tasks, as well as for the study of pathologies that alter the airways structure. In this paper, we present an efficient segmentation and reconstruction algorithm which simultaneously segments and reconstructs the bronchial tree, while providing the length and mean radius of each airway segment. A locally adaptive intensity threshold is used to account for the low signal to noise ratio and strong artifacts present in micro-CT images. We validate our method by comparing it with manual segmentations of 10 different scans, obtaining an average true positive volume fraction of 85.52% with a false positive volume fraction of 5.04%.

Keywords: Airway segmentation, micro-CT, mouse, airway measurement

1. INTRODUCTION

Several studies have shown the potential impact of high resolution Computed Tomography (micro-CT) for the study of small animal models of lung disease.[1,2] Automatic lung segmentation in micro-CT images should allow for accurate and reproducible quantification of lung disease. Specifically, lung airway-tree segmentation has many potential applications: First, segmenting the airways facilitates a more accurate segmentation of the lungs, by simply separating the airways from the lung parenchyma. This is of particular interest when studying pathologies that affect lung parenchyma, such as emphysema or fibrosis.[2] Alternatively, airways can also be used as a reference for image registration, which might be useful in atlas-based whole lung segmentation. Finally, segmenting the airways is a necessary step to study diseases that affect their morphology or integrity.

Several approaches exist for segmenting the human airways in Computed Tomography (CT) images. For instance, Aykac et al.[3] proposed a two-step approach, in which airway lumens are first identified in 2-D slices using grayscale morphological reconstruction and then connected with each other to create a 3-D tree. In a subsequent work, Tschirren et al.[4] employed a fuzzy-connectivity algorithm. This algorithm was applied not on the whole image at the same time, but on adaptive regions of interest that followed the airway branches that had been already segmented. This approach limited the probability of leakages into the parenchyma. In a recent work, Graham et al.[5] search for airway sections over the whole lung and connect them to the tree using a graph partitioning algorithm. These are only a few examples of the large variety algorithms designed to segment human airways in CT images. However, due to the low Signal to Noise Ratio (SNR) and strong artifacts of micro-CT images,[6] these algorithms can not be directly applied to small animal CT data.

To the best of our knowledge, only two methods have been proposed for segmenting murine airways in micro-CT images. Chaturvedi et al.[7] imaged silicon casts of excised mice lungs, which were segmented using an interactive region growing algorithm. This algorithm required moderate operator interaction and was not used to segment the lungs of live animals. Shi et al.[8] proposed a fully automatic method, based on the search of airway lumens in 2-D slices followed by 3-D tree reconstruction. The main drawback of their method is the fact that it is based on the search of candidates in 2-D. This may cause problems depending on the orientation of the airways, which in turn affects the way they appear in the images. Moreover, reported computation times were fairly high (about 30 minutes for each scan).

Medical Imaging 2009: Biomedical Applications in Molecular, Structural, and Functional Imaging, edited by Xiaoping P. Hu, Anne V. Clough, Proc. of SPIE Vol. 7262, 72620B · © 2009 SPIE · CCC code: 1605-7422/09/$18 · doi: 10.1117/12.811554

In this article, we adopt the framework proposed by Bülow et al.,[9] which has been successfully used in human airway segmentation.[10,11] The framework consists of a propagating wavefront which creates segments as it grows within the airways. There are some rules to accept voxels, as well as to accept a propagation step and a complete segment. It has the advantage that, along with the segmentation, it gives the length and mean radius of each segment of the airway. We have adapted and added new features to the framework to succesfully segment mouse airways in micro-CT images. Segmentations were validated on 10 scans, by comparing automated results to manual segmentations on every fifth transversal slice.

The outline of the article is the following. In the methods section, technical details about the segmentation and reconstruction algorithm are given, as well as about the image acquisition protocol. In section 3, results from comparing automatic and manual segmentation are shown. The method and results are discussed in section 4 and a final conclusion is given in section 5 .

2. METHOD

2.1 Filtering

Due to the small voxel size -tens of microns- and the limited radiation dose used in *in-vivo* experiments, micro-CT images display high levels of noise and artifacts. This justifies the need of a filtering step before any automatic image processing or analysis. We chose a 3-D grayscale closing by reconstruction filter with a spherical structuring element of radius 1.[12] The reason for this choice was that the 2-D version of this filter was reported to yield positive results in the previous work by Shi et al.[8] The radius was selected because it represented a good trade-off between noise removal and contour information preservation.

2.2 Airway tree segmentation and reconstruction

The used framework has been explained in detail in two papers by Bülow et al.[9] and Schlathölter et al.[10] A block diagram summarizing the main execution flow is shown in Fig. 1. A *segment* is a set of points, that ideally corresponds to a single airway branch. Initialized but yet unprocessed segments are stored in a sorted *segment queue*. This queue is a *Last-In, Last-Out* (LILO) list, to make sure that branches from upper airways are processed first.

The segmentation and reconstruction process occurs simultaneously. When a bifurcation is detected while a segment is growing, the current segment propagation is stopped and the new segments are added to the end of the segment queue. The next segment to be grown is taken from beginning of the queue.

The rest of relevant aspects of the algorithm, which include inizialization, wavefront propagation, voxel acceptance, propagation evaluation and segment evaluation, will be outlined in this subsection.

2.2.1 Initialization

The initial wavefront is created from a seed point which, in the current implementation of the algorithm, must be manually placed in the first transversal slice. The *confidence connected* filter of the Insight Toolkit[14] is used to segment the trachea in the first slice. This is a region growing algorithm that uses the statistics of the already segmented region to define the growing criterion. A voxel is included in the segmented region if its intensity is within the following limits: $[m - \beta\sigma, m + \beta\sigma]$, where β is a factor defined by the user, and m and σ are the mean and the standard deviation of the segmented region intensities. The growing process is repeated iteratively until a given iteration number is reached. In this work, the initial neighborhood was set to 3, the number of iterations to 5, and the multiplier β to 3.

2.2.2 Wavefront propagation

In the original work by Bülow et al.[9] the wavefront propagates using a fast marching method. We adopt the solution employed by van Ginneken et al.,[11] that uses a simple region growing algorithm, for its straighforward implementation and rapid execution time. To make sure that the wavefront is dome-shaped and that the bifurcations are detected properly, the growth is limited to a *confinement sphere*. The radius of the sphere is 2.5 times the radius of the current wavefront and its center is located in the previous wavefront center of gravity.

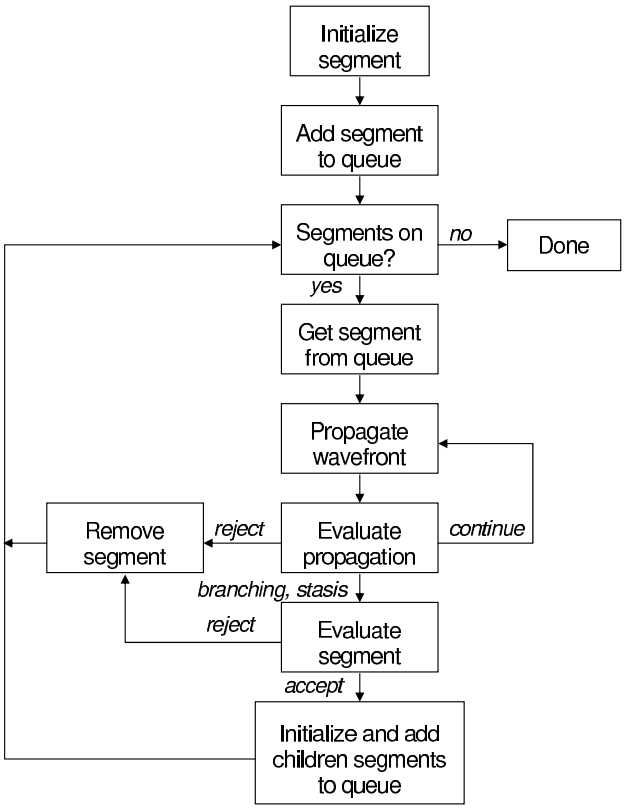

Figure 1. Block diagram of general tree segmentation and reconstruction framework. (Adapted from Baggerman[13])

2.2.3 Voxel acceptance criteria

In each propagation step, voxels in contact with wavefront voxels are candidate to be added to the current segment and become new wavefront segments. There are two criteria that a voxel must fulfill before being accepted: the similar intensity condition and the low gradient condition. The similar intensity condition is given by a variable upper threshold, which accounts for the large variability in image intensities observable in micro-CT images. In other words, the low SNR and the strong artifacts, cause the airway branches to have different intensities depending on their location. Therefore, it becomes necessary to have a threshold that varies within the same image. We define the variable threshold as:

$$T = \mu_l + \alpha \cdot max(\sigma_p, \sigma_{gp}), \tag{1}$$

where μ_l is the mean intensity of the current segment (l stands for *local*), α is a tunable parameter set to 1.4, and σ_p and σ_{gp} are the standard deviations of the intensity values of the voxels in the parent and grandparent segments of the current one. The largest of both is taken, to avoid very small σ-s in case of a short or very homogeneous segment, which would lead to a too low threshold T. Intensities are averaged in a neighborhood of 27 voxels around the voxels of interest to minimize the effect of noise.

For the low gradient condition, the three-dimensional Sobel gradient is computed and voxels are rejected if their Sobel gradient value exceeds 1800. This way segmentation leakage from the airways and into the lungs is avoided.

2.2.4 Propagation evaluation

There are two criteria to accept or reject a propagation step. The first controls the current size of the wavefront, and prevents it from growing too much. This is implemented by not allowing wavefronts to be larger than the

wavefronts in their parent segments. To account for noise and anatomical irregularities, propagation is stopped if the current wavefront radius is larger than:

$$\gamma \cdot \frac{min(all\ ancestor\ radii) + mean(radii\ in\ ancestor\ with\ min\ radius)}{2}, \tag{2}$$

where γ is a tunable parameter set to 2 to allow certain growth, $min(all\ ancestor\ radii)$ is the minimum radius in all ancestors of the current segment and $mean(radii\ in\ ancestor\ with\ min\ radius)$ is the mean value of wavefront radius in the ancestor containing the minimum radius. The latter is averaged with the smallest radius because the smallest radius alone resulted in a too noisy measure, which limited propagation in some cases.

The second propagation evaluation rule refers to the number of neighbor segments. This number is limited to 2, because the number of neighbors is computed before the current segment has stopped its propagation and its children segments have been initialized. A number greater than 2 generally indicates that several small segments are growing next to each other, which is a common indicator of leakage.

2.2.5 Segment evaluation

A combined rule is used to accept or reject fully grown segments. A segment is considered to be fully grown when a bifurcation of the wavefront is detected or it can not grow further. To this end, the Growth Rate (GR) and the Compactness[15] (C) of the segment are evaluated. The growth rate is given by:

$$\mathrm{GR} = \frac{1}{n}\sum_{i=1}^{n}\frac{|W_i|}{|W_{i-1}|}, \tag{3}$$

where n is the number of propagation steps in the segment and $|W_i|$ is the number of voxels of the wavefront at propagation step i. Thus, a GR larger than one indicates that the segment has grown during propagation.

We use the definition of object compactness by Bribiesca[15] for 3-D shapes. In a solid volume of n voxels, its discrete compactness is given by:

$$\mathrm{C} = \frac{n - A/6}{n - (\sqrt[3]{n})^2}, \tag{4}$$

where A is the area of the enclosing surface, and corresponds to the sum of the areas of the external plane polygons of the voxels which form the visible faces of the solid. Low compactness is related to a specific kind of leakage, where the resulting incorrect segment has a spongy shape. This specific leakage does not present a high GR, but they can be detected thanks to their low C. Combining C and GR, we defined a combined rule by which a segment is rejected if $GR > 1.2$; $GR > 1$ and $C < 0.7$; or $GR < 1$ and $C < 0.6$.

2.3 Image acquisition

Our imaging protocol is inspired by the work of Namati et al.[16] Animals were anesthetized with an intraperitoneal injection of 90 mg/kg ketamine and 10 mg/kg xylacine. Endotracheal intubation was performed on anesthesized animals using the BioLite system (Biotex, Houston, Texas), to illuminate the trachea with a fiber optic stylet. After intubation, animals were connected to an Ugo Basile 7025 rodent ventilator (Ugo Basile, Comerio, Italy). A custom-made controller was used to set the respiration cycle as follows: 3 normal breaths at a rate of 85 breaths/min followed by a stop -apnea- of 700 ms at full lungs. An injection of 0.05 mg/kg of Pancuronium bromide (Organon, Oss, The Netherlands) was required to completely stop animal movement.

Images were acquired with a Micro-CAT II scanner (Siemens Pre-Clinical Solutions, Knoxville, Tennesee), with a source voltage of 80 kVp and a current of 500 μA. The exposure time per projection was 450 ms and each projection was acquired during the 700 ms full inspiration apneae. 700 projections per scan were acquired. This resulted in images of 640 slices with 1024×1024 voxels per slice, and an isotropic resolution of 46 μm.

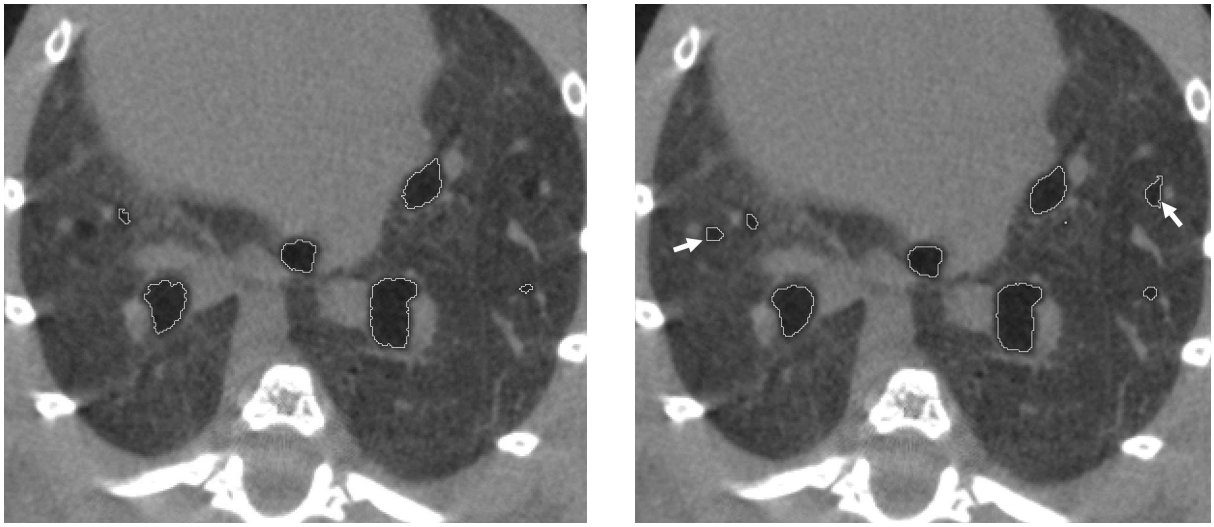

(a) Manual segmentation (b) Automatic segmentation

Figure 2. Axial slice comparing manual (a) and automatic (b) segmentations. Two correct airway sections have been missed by the manual segmentation and correctly labeled by the automatic segmentation (pointed with an arrow in (b)).

3. RESULTS

Ten scans of ICR mice were used for algorithm validation. In those scans, one every fifth transversal slices was interactively segmented using the Amira software (Visage Imaging, Fürth, Germany). To this end, a seed was placed inside every visible airway and region growing was applied. The upper threshold for region growing was modified to adjust to airway characteristics in each case. In occasions in which this approach failed (mainly due to leakage in the parenchyma) the airway limits were delineated manually. The whole process took around 90 minutes per scan.

To assess the accuracy of our segmentation method, we computed the True Positive Volume Fraction (TPVF) and False Positive Volume Fraction (FPVF) as defined in the work of Shi et al.:[8]

$$\text{TPFV} = \frac{|S_A \cap S_M|}{|S_M|}, \ \text{FPFV} = \frac{|S_A - S_M|}{|S_M|}, \tag{5}$$

where S_A is the automatic segmentation, S_M is the manual segmentation, $|S_A \cap S_M|$ represents the intersection between the two segmentations and $|S_A - S_M|$ represents the pixels that where marked as airway by the automatic algorithm but not by the manual segmentation.

The drawback of this definition of FPVF is that it can yield results larger than one, but there is no consensus on which value should be selected for the denominator.[17] Another option would be to use the union of the segmentations $|S_A \cup S_M|$. We decided to use the same definition used in Shi et al.[8] to allow comparison of results.

The resulting mean values for TPVF and FPVF were 85.52% and 5.08% respectively, with standard deviations of 2.90% and 2.60%. It must be noted that, as in the work by Shi et al.,[8] manual segmentations are not perfect and some real airways can be missed. An example with two airway branches missed by the manual segmentation and detected by the automatic algorithm is illustrated in Figs. 2a and 2b. This effect increases the FPVF artificially.

In Fig. 3, two sample renderings of the automatically segmented airway tree can be seen. Different branches are shown in different gray levels.

The computation time per image was around 60 seconds for image segmentation and reconstruction, including 30 seconds for image filtering.

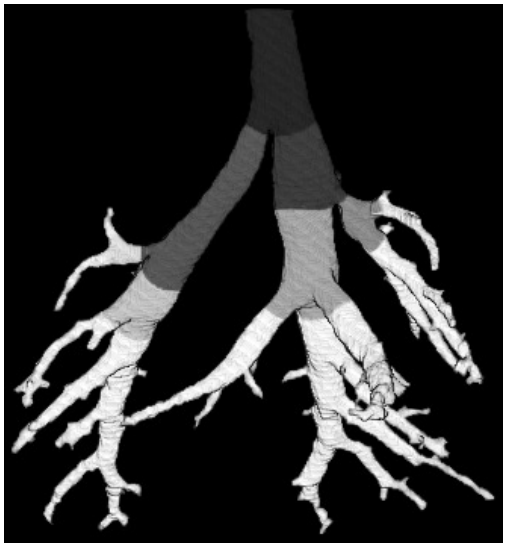

(a) Volume rendering 1

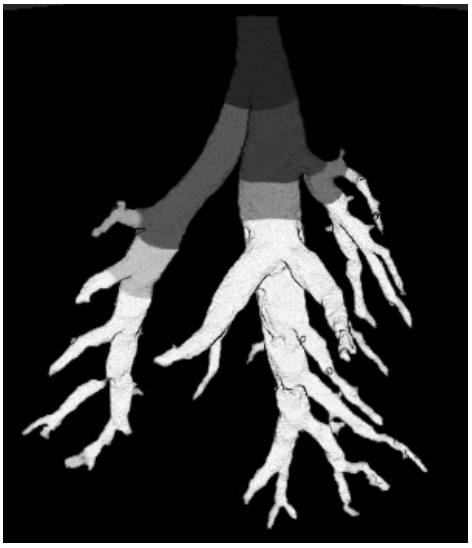

(b) Volume rendering 2

Figure 3. Two volume renderings of two of the 10 segmentations. Only main segments are shown in different gray levels.

4. DISCUSSION

In-vivo micro-CT images of the mouse chest generally have low SNR, due to high-noise associated to the low radiation dose required for in-vivo scans, to movement and reconstruction related artifacts, and to the small voxel size. In our case, movement artifacts were greatly reduced thanks to the ventilator-controlled acquisition protocol, but radiation dose and small voxel size impose a limit to the improvement in SNR.[6] Therefore, any image analysis algorithm to be used on these images must be robust against noise. We have developed on the tree-like structure segmentation and reconstruction algorithm introduced by Bülow et al.[9] In particular, we have introduced new features (such as a variable threshold) that make the algorithm more appropriate to the airway segmentation on this kind of image.

A basic characteristic of the original framework is that the region growing is based on a Fast Marching algorithm. For simplicity, we have used a simple region growing algorithm with a confinement sphere. The radius of the sphere varies together with the wavefront. This approach has given satisfactory results. However, it will be interesting to see the effect of applying a Fast Marching region growing in the overall performance. We plan to do this as part of our future work.

The proposed algorithm gives not only a binary segmentation of the airway tree, but separates each branch too. Thus, the topology of the tree can be easily traced as well: the parent and children of each branch are identified. We believe that this is a major advantage of this technique when compared to other algorithms that simply segment the tree, for two reasons. Firstly, topological information can be used to help segmentation, for instance by comparing the current segment with its ancestors' radius or by checking the number of neighbor segments. Secondly, it eliminates the need for an extra skeletonization step. Moreover, our algorithm provides with measurements of the length and mean radius of the segments of each airway.

Another advantage of the technique is its rapid execution: it runs in less than one minute. Considering that around one half of this time is spent in image filtering, studying alternative -faster- filtering algorithms might be another interesting step for future work.

The evaluation and validation of automatic segmentation algorithms is not an straighforward task.[17] In this case, we have compared the automatic segmentations with manual segmentations performed every fifth slice. Manual segmentation of mice airways in micro-CT images is a time consuming task which can result in multiple errors. The most common error was to miss small airways, some of which were detected by the automatic method, thus resulting in an incorrectly higher FPVF. A second view correcting for this errors could decrease

this evaluation error. Another option would be to add a second observer, which would give an idea of the human inter-observer variability.

Segmenting and reconstructing the airway trees in *in-vivo* images of mice lungs has many potential applications. First, it will allow for a more accurate segmentation of the lungs. This is of special relevance when studying disease models that affect the density of the lung as seen on micro-CT images, such as emphysema. Not removing the airways from the lungs might lead to inaccurate volumetric quantification. Segmented airways could also be used as a reference for image registration in atlas-based segmentation or in follow-up studies. Finally, the segmentation and reconstruction can be used to study diseases that affect airway morphology or integrity.

5. CONCLUSIONS

We have presented a fast and robust algorithm for mouse airway segmentation and reconstruction in micro-CT images. The algorithm not only segments the bronchial tree, but also provides the length and mean radius of each segment. We believe that this has many applications both for further image analysis and for the study of animal models of lung disease.

REFERENCES

[1] Recheis, W., McLennan, G., Ross, A. F., and Hoffman, E. A., [*Molecular Imaging of the Lungs*], ch. Imaging the mouse lung with micro-CT, Taylor and Francis (2005).

[2] Froese, A. R., Ask, K., Labiris, R., Farncombe, T., Warburton, D., Inman, M. D., Gauldie, J., and Kolb, M., "Three-dimensional computed tomography imaging in an animal model of emphysema," *European Respiratory Journal* **30**(6), 1082–1089 (2007).

[3] Aykac, D., Hoffman, E., McLennan, G., and Reinhardt, J., "Segmentation and analysis of the human airway tree from three-dimensional X-ray CT images," *IEEE Transactions on Medical Imaging,* **22**, 940–950 (August 2003).

[4] Tschirren, J., Hoffman, E., McLennan, G., and Sonka, M., "Intrathoracic airway trees: segmentation and airway morphology analysis from low-dose CT scans," *IEEE Transactions on Medical Imaging* **24**, 1529–1539 (December 2005).

[5] Graham, M. W., Gibbs, J. D., and Higgins, W. E., "Robust system for human airway-tree segmentation," *Medical Imaging 2008: Image Processing* **6914**(1), 69141J, SPIE (2008).

[6] Ford, N. L., Thornton, M. M., and Holdsworth, D. W., "Fundamental image quality limits for microcomputed tomography in small animals," *Medical Physics* **30**(11), 2869–2877 (2003).

[7] Chaturvedi, A. and Lee, Z., "Three-dimensional segmentation and skeletonization to build an airway tree data structure for small animals," *Physics in Medicine and Biology* **50**(7), 1405–1419 (2005).

[8] Shi, L., Thiesse, J., McLennan, G., Hoffman, E. A., and Reinhardt, J. M., "Three-dimensional murine airway segmentation in micro-CT images," *Medical Imaging 2007: Physiology, Function, and Structure from Medical Images* **6511**(1), 651105, SPIE (2007).

[9] Bülow, T., Lorenz, C., and Renisch, S., [*Medical Image Computing and Computer-Assisted Intervention MICCAI 2004*], ch. A general framework for tree segmentation and reconstruction from medical volume data, Springer Berlin / Heidelberg (2004).

[10] Schlathölter, T., Lorenz, C., Carlsen, I. C., Renisch, S., and Deschamps, T., "Simultaneous segmentation and tree reconstruction of the airways for virtual bronchoscopy," *Medical Imaging 2002: Image Processing* **4684**(1), 103–113, SPIE (2002).

[11] van Ginneken, B., Baggerman, W., and van Rikxoort, E. M., [*Medical Image Computing and Computer-Assisted Intervention MICCAI 2008*], ch. Robust segmentation and anatomical labeling of the airway tree from thoracic CT scans, 219.226, Springer Berlin / Heidelberg (2008).

[12] Vincent, L., "Morphological grayscale reconstruction in image analysis: applications and efficient algorithms," *IEEE Transactions on Image Processing* **2**, 176–201 (February 1993).

[13] Baggerman, W., *Extraction of bronchial and aortic tree using a generic framework*, Master's thesis, Image Sciences Institute, University Medical Center Utrecht (2007).

[14] Kitware, *ITK Software Guide, Online: www.itk.org/ItkSoftwareGuide.pdf.*
[15] Bribiesca, E., "An easy measure of compactness for 2D and 3D shapes," *Pattern Recogn.* **41**(2), 543–554 (2008).
[16] Namati, E., Chon, D., Thiesse, J., Hoffman, E. A., de Ryk, J., Ross, A., and McLennan, G., "In vivo micro-CT lung imaging via a computer-controlled intermittent iso-pressure breath hold (IIBH) technique," *Physics in Medicine and Biology* **51**(23), 6061–6075 (2006).
[17] Udupa, J. K., LeBlanc, V. R., Zhuge, Y., Imielinska, C., Schmidt, H., Currie, L. M., Hirsch, B. E., and Woodburn, J., "A framework for evaluating image segmentation algorithms," *Computerized Medical Imaging and Graphics* **30**, 75–87 (March 2006).